

[Fe II] and H₂ filaments in the Supernova Remnant G11.2–0.3: Supernova Ejecta and Presupernova Circumstellar Wind

Bon-Chul Koo

*Astronomy Program, Department of Physics and Astronomy, Seoul National University,
Seoul 151-747, Korea*

koo@astrohi.snu.ac.kr

Dae-Sik Moon¹

*Robert A. Millikan Fellow, Division of Physics, Mathematics, and Astronomy, California
Institute of Technology, MC 103-33, Pasadena, CA 91125*

moon@srl.caltech.edu

Ho-Gyu Lee and Jae-Joon Lee

*Astronomy Program, Department of Physics and Astronomy, Seoul National University,
Seoul 151-747, Korea*

hglee@astro.snu.ac.kr, jjlee@astro.snu.ac.kr

Keith Matthews

California Institute of Technology, Downs Lab, MS 320-47, Pasadena, CA 91125

kym@caltech.edu

ABSTRACT

We present the results of near-infrared imaging and spectroscopic observations of the young, core-collapse supernova remnant (SNR) G11.2–0.3. In the [Fe II] 1.644 μm image, we first discover long, clumpy [Fe II] filaments within the radio shell of the SNR, together with some faint, knotty features in the interior of the remnant. The filaments are thick and roughly symmetric with respect to the NE-SW elongation axis of the central pulsar wind nebula. We have detected

¹Department of Astronomy and Astrophysics, University of Toronto, Toronto, ON M5S 3H4, Canada

several [Fe II] lines and H α Br γ line toward the peak position of the bright southeastern [Fe II] filament. The derived extinction is large ($A_V = 13$ mag) and it is the brightest [Fe II] 1.644 μm filament detected toward SNRs to date. By analyzing two [Fe II] 1.644 μm images obtained in 2.2 yrs apart, we detect a proper motion corresponding to an expansion rate of $0.''035 \pm 0.''013 \text{ yr}^{-1}$ ($830 \pm 310 \text{ km s}^{-1}$). In addition to the [Fe II] features, we also discover two small H $_2$ 2.122 μm filaments. One is bright and along the SE boundary of the radio shell, while the other is faint and just *outside* of its NE boundary. We have detected H $_2$ (2-1) S(3) line toward the former filament and derive an excitation temperature of 2,100 K. We suggest that the H $_2$ filaments are dense clumps in a presupernova circumstellar wind swept up by the SNR shock while the [Fe II] filaments are probably composed of both shocked wind material and shocked supernova (SN) ejecta. The distribution of [Fe II] filaments may indicate that the SN explosion in G11.2–0.3 was asymmetric as in Cassiopeia A. Our results support the suggestion that G11.2–0.3 is a remnant of a SN IIL/b interacting with a dense red supergiant wind.

Subject headings: ISM: individual (G11.2–0.3) — infrared: ISM — shock waves — supernovae: general — supernova remnants

1. Introduction

G11.2–0.3 is a composite-type SNR with a central pulsar wind nebula (PWN) surrounded by a circular shell. The shell is bright both in radio and X-rays, and has an outer diameter of $4'$ and a thickness of $0.'5$ (Green et al. 1988; Roberts et al. 2003). The shell is clumpy with several clumps protruding its outer boundary. The bright radio shell with high circular symmetry indicates that the remnant is young and it is thought to be the best candidate for the possible historical supernova of AD 386 (Stephenson & Green 2002). The PWN with an associated pulsar was discovered at the very center of the remnant in X-rays with *ASCA*, and later its detailed structure was studied with the Chandra X-ray Observatory (Vasisht et al. 1996; Kaspi et al. 2001; Roberts et al. 2003, and references therein). The PWN is elongated along the NE-SW direction with a total extent of $1'$, and appears to be surrounded by a radio synchrotron nebula with similar extent and shape. The distance to G11.2–0.3 determined from HI absorption is 5 kpc (Green et al. 1988).

The overall morphology of G11.2–0.3 resembles Cassiopeia A (Cas A). Both have a thick, bright, and clumpy shell, although the shell of Cas A is much brighter than that

of G11.2–0.3, i.e., 2720 Jy vs 22 Jy at 1 GHz (Green 2004)¹. At a distance of 3.4 kpc, the outer radius of Cas A shell is 2.0 pc and its expansion velocity is 4,000–6,500 km s^{−1} (e.g., Fesen & Gunderson 1996), while they are 2.9 pc and $\sim 1,000$ km s^{−1} for G11.2–0.3. Cas A has a faint 5′ (or 2.5 pc)-diameter plateau extending beyond the bright shell (e.g., Hwang et al. 2004). The plateau represents swept-up circumstellar (or ambient) medium while the bright shell is thought to be mainly the ejecta swept up by a reverse shock. Such plateau has not been detected in G11.2–0.3. Chevalier (2005) classified both Cas A and G11.2–0.3 into SN IIL/b category which has a red supergiant (RSG) progenitor star with some H envelope but most lost (cf. Hwang & Laming 2003; Young et al. 2006). Detailed observations have revealed that the explosion of Cas A was turbulent and asymmetric and that the ejecta is now interacting with a clumpy circumstellar wind (see Hwang et al. 2004; Chevalier & Oishi 2003, and references therein). However, very little is known about the explosion and the interaction of the 1620(?) yr-old G11.2–0.3 despite its close similarity to Cas A.

In this paper, we report the discovery and detailed studies of [Fe II] and H₂ filaments in the SNR G11.2–0.3 using near-infrared (IR) imaging and spectroscopic observations. Although the recent mid-IR data obtained with the Spitzer Space Telescope show the presence of very faint wispy emission close to its SE boundary (Lee 2005; Reach et al. 2006), our near-IR observations reveal much more prominent and extended features both at the boundary and interior of the remnant, which provide important clues on the origin and evolution of G11.2–0.3.

2. Observations

We carried out near-IR imaging observations of the SNR G11.2-0.3 with Wide-field Infrared Camera (WIRC) on the Palomar 5-m Hale telescope using several narrow- and broad-band filters in 2003 June and 2005 August (Table 1). WIRC is equipped with a Rockwell Science Hawaii II HgCdTe 2K infrared focal plane array, covering $\sim 8.5 \times 8.5$ field of view with 0."25 pixels scale. For the basic data reduction, we subtracted dark and sky background from each individual dithered image and then normalized it by a flat image. We finally combined the individual images to make a final image. The seeing was typically 0."8–1" over the observations. We obtained the flux calibration of our narrow-band filter (i.e., [Fe II] and H₂) images using the H (for [Fe II] 1.644 μ m) and Ks (for H₂ 2.122 μ m) band magnitudes of ≥ 20 nearby isolated, unsaturated 2MASS stars. For this, we first

¹Also available at <http://www.mrao.cam.ac.uk/surveys/snrs/>.

converted the 2MASS magnitudes to fluxes (Cohen, Wheaton, Megeath 2003), and then obtained the fluxes of the [Fe II] and H₂ emission after we deconvolved the responsivities of both WIRC ([Fe II] and H₂) and 2MASS (*H* and *K_s*) filters. The overall uncertainty in the flux calibration is less than 10%. We attribute the major source of uncertainty to the different band response of each filter as the uncertainty in photometry itself is typically a few percent. For the astrometric solutions of our images, we used all the cataloged 2MASS stars in the field, and found that they are consistent with that of 2MASS with rms uncertainty of 0."15.

After identifying several emission-line features in the aforementioned imaging observations, we have carried out follow-up spectroscopic observations of them using Long-slit Near-IR Spectrograph of the Palomar 5-m Hale Telescope (Larkin et al. 1996) in 2005 August. The spectrograph has a 256 × 256 pixel HgCdTe NICMOS 3 array with a fixed slit of 38" length. We placed the slit along the bright [Fe II] and H₂ filaments crossing their peak positions. Toward the [Fe II] filament, four spectra around 1.25, 1.52, 1.63 μm (for [Fe II] emission), and 2.16 μm (for H I Brγ) were obtained, while, toward the H₂ filament, one spectrum around 2.11 μm was obtained. Over the observations, the slit width was fixed to be 1", resulting in spectroscopic resolution of 650–850 with 0.06–0.12 μm usable wavelength coverage. For all the obtained spectra, the individual exposure time was 300 s with the same amount of exposure of nearby sky for sky background subtraction. For the [Fe II] lines, we performed the exposure twice (with different sky positions, but the same source position), and combined them, while, for the H₂ line, we performed the exposure only once.

Just after the source observations, we obtained the spectra of the G3V star HR 8545, which was at the similar airmass of the source by uniformly illuminating the slit using the f/70 chopping secondary of the telescope. We then divided the source spectra by those of HR 8545 and multiplied by a blackbody radiation curve of the G3V star temperature, which is equivalent to simultaneous flat fielding and atmospheric opacity correction. G stars, however, have numerous intrinsic (absorption) features, so that this procedure could inflate the intensities of emission lines if they fall on these stellar features. We have estimated the errors using the G2V solar spectrum (Livingston & Wallace 1991)² as a template of our reference star HR 8545 (cf. Maiolino, Rieke, & Rieke 1996; Vacca, Cushing, & Rayner 2003). The estimated errors in the observed line fluxes are ≤ 5% for all lines except Brγ line for which it is 10%. The resulting errors in the line ratios, which are used for the derivation of physical parameters, are ≤ 2% except for the Brγ/[Fe II] 1.644 μm ratio for which it is 7%. These calibration errors are all less than their statistical (1σ) errors (see Table 2). Another

²Also available at <http://diglib.nso.edu/contents.html>.

source of error is different atmospheric condition. All spectra of the source and HR 8545 were obtained at air mass of 1.6–1.8 except the H₂ spectra of the source which was obtained at an air mass of 2.27. There is a strong atmospheric CO₂ absorption line between 2.05 and 2.08 μm, and the different airmasses can give an error in the intensity of H₂ (2–1) S(3) line at 2.0735 μm. According to Hanson, Conti, & Rieke (1996), the error is about 2% when the air masses differ by 0.3, so that it would be $\lesssim 5\%$ for our H₂ (2–1) S(3) line. Again, this is less than the (1σ) statistical error. We therefore consider that the uncertainty due to the calibration errors is less than the statistical errors quoted in this paper (Table 2). For the wavelength solutions of the spectra, we used the OH sky lines (Rousselot et al. 2000).

3. Results

Fig. 1 (right) is our three-color image representing the near-IR [Fe II] 1.644 μm (B), H₂ 2.122 μm (G), and Brγ 2.166 μm (R) emission of the SNR G11.2–0.3. We also show an 1.4 GHz VLA image for comparison which was obtained by Green et al. (1988) in 1984–85 with 3'' resolution. Note that the expansion rate of G11.2–0.3 at 1.4 GHz is $0.''057 \pm 0.''012 \text{ yr}^{-1}$ (Tam & Roberts 2003) which amounts to $\sim 1''$ over the last 20 years (see also §3.3). The near-IR emission features in Fig. 1 can be summarized as follows: (1) an extended ($\sim 2.''5$), bright [Fe II] (blue) filament along the SE radio shell; (2) some faint, knotty [Fe II] emission features along the NW radio shell as well as in the interior of the source; (3) a small (30''), bright H₂ (green) filament along the outer boundary of the source in the SE; (4) another small, faint H₂ filament outside the NE boundary of the source. Overall the [Fe II] filaments are located either within the radio shell or inside of the source, while the H₂ filaments are along the radio boundary or even outside of it. We have not found any apparent Brγ filament in our rather shallow imaging observation, although we have detected faint Brγ line emission toward the [Fe II] peak position in our spectroscopic observation. In the following, we summarize the results on the [Fe II] and H₂ emission features.

3.1. [Fe II] 1.644 μm emission

3.1.1. Photometry

In order to see the [Fe II] emission features more clearly, we have produced an ‘star-subtracted’ image (Fig. 2). We first performed PSF photometry of H-cont and [Fe II] 1.644 μm images, and removed stars in the [Fe II] 1.644 μm image if they had corresponding ones in the H-cont image. This PSF photometric subtraction left residuals around bright

stars which we masked out. The faint stars, which were not removed by the PSF subtraction because the H-cont image is not as deep as that of [Fe II], were then removed by subtraction of median value of 15×15 nearby pixels. Fig. 2 is the final star-subtracted image where we can see the detailed features of [Fe II] emission more clearly.

As in Fig. 1 (right), the extended filament within the southeastern SNR shell, [Fe II]-SE filament hereafter, is most prominent. The filament is composed of two bright, $30''$ -long, elongated segments in the middle and two clumpy segments at the ends. The one at the southern end is a little bit apart from the other three. The total extent of the filament is $\sim 2.5'$. The filament is not very thin but has a width of $\lesssim 10''$. Fig. 3 shows a detailed structure of the filament, where we have just masked out stars using the K-cont image in order to avoid any possible artifacts associated with the PSF photometric subtraction. We can see that the filament has a very good correlation with the radio shell both in morphology and brightness. The peak [Fe II] $1.644 \mu\text{m}$ surface brightness of the filament is $1.9 \pm 0.2 \times 10^{-3} \text{ ergs cm}^{-2} \text{ s}^{-1} \text{ sr}^{-1}$, which is larger than any previously reported brightness of [Fe II] $1.644 \mu\text{m}$ filaments in other remnants, e.g., $1.1\text{--}3 \times 10^{-4} \text{ ergs cm}^{-2} \text{ s}^{-1} \text{ sr}^{-1}$ in IC 443 and Crab (Graham, Wright, & Longmore 1987, 1990) or $1.5 \times 10^{-3} \text{ ergs cm}^{-2} \text{ s}^{-1} \text{ sr}^{-1}$ in RCW103 (Oliva, Moorwood, & Danziger 1989).

On the opposite side of the SE filament lies another long ($\sim 2.5'$) filament within the northwestern SNR shell (Fig. 4). This filament ([Fe II]-NW filament) is relatively faint and appears to be clumpy. It has little correlation with the radio emission. We note that [Fe II]-SE and NW filaments lie roughly symmetric with respect to the line of position angle $\approx 60^\circ$, which is close to the inclination of the central PWN of G11.2–0.3 in X-ray (Roberts et al. 2003). In addition to these two extended filaments, some faint, knotty emission features are also seen in the interior of the remnant, particularly in the southern area (Fig. 5). These features spread over an area of $\sim 2'$ extent and filamentary, with some of them having a partial ring-like structure. There are also several bright clumps of $\sim 5''$ size. Most of the clumps appear to be connected to the filaments, although some are rather isolated. The brightnesses of these central emission features and NW filament are $\lesssim 3 \times 10^{-4} \text{ ergs cm}^{-2} \text{ s}^{-1} \text{ sr}^{-1}$. The observed total [Fe II] $1.644 \mu\text{m}$ flux is estimated to be $1.1 \pm 0.2 \times 10^{-11} \text{ erg cm}^{-2} \text{ s}^{-1}$, $76 \pm 12\%$ of which is from the SE filament.

3.1.2. Spectroscopy

We have detected several [Fe II] lines toward the peak position of the [Fe II]-SE filament ([Fe II]-pk1). Table 2 summarizes the detected lines and their relative strengths, and Fig. 6 shows the spectra. [Fe II] $1.257 \mu\text{m}$ and [Fe II] $1.644 \mu\text{m}$ lines originate from the same upper

level, so that their unreddened flux ratio is fixed by relative Einstein A coefficients which is 1.04 according to Quinet, Le Dourneuf, & Zeippen (1996). Toward [Fe II]-pk1, the ratio is 0.31, which implies $A_V = 13$ mag ($A_{1.644\mu\text{m}} = 2.43$ mag) or H-nuclei column density of $2.49 \pm 0.07 \times 10^{22}$ cm $^{-2}$ using the extinction cross section of the carbonaceous-silicate model for interstellar dust with $R_V = 3.1$ of Draine (2003)³. This is a little larger than the column density to the remnant derived from X-ray observations $(1.7-2.4) \times 10^{22}$ cm $^{-2}$ (Roberts et al. 2003). We note that the numerical values of the Einstein A coefficients for near-IR [Fe II] lines in the literature differ as much as 50%: using the values of Nussbaumer & Storey (1988), the expected [Fe II] 1.257 μm to [Fe II] 1.644 μm line-intensity ratio is 1.36, while Smith & Hartigan (2006) empirically derived 1.49 from their spectroscopy of P Cyg. If the intrinsic ratio is 1.36 or 1.49, we obtain a little (20–30%) higher column density. We adopt the A -values of Quinet, Le Dourneuf, & Zeippen (1996) in this paper which yield a column density closer to the X-ray one. According to Hartigan, Raymond, & Pierson (2004), they also yield extinction more consistent with optical spectroscopic result for a protostellar jet.

The ratios of the other three lines, e.g., [Fe II] 1.534 μm , 1.600 μm , and 1.664 μm , to [Fe II] 1.644 μm are good indicators of electron density (e.g., Oliva, Moorwood, & Danziger 1990). We solved the rate equation using the atomic parameters assembled by CLOUDY (version C05.05, Ferland et al. 1998) which adopts the Einstein A coefficients of Quinet, Le Dourneuf, & Zeippen (1996) and collision strengths of Padhan & Zhang (1993) and Zhang & Pradhan (1995). We have included 16 levels which is enough at temperatures of our interest ($\lesssim 10^4$ K). We consider only the collisions with electrons, neglecting those with atomic hydrogen, even if the degree of ionization of the emitting region could be low (see § 4.2). This should be acceptable since the rate coefficients for atomic hydrogen collisions are more than two orders of magnitude smaller than those for electron collisions (Hollenbach & McKee 1989). The ratios of 1.534 μm and 1.664 μm lines yield consistent results, e.g., $6,000 \pm 400$ cm $^{-3}$ and $5,900 \pm 400$ cm $^{-3}$, while 1.600 μm line ratio yields a little higher density ($7,800 \pm 400$ cm $^{-3}$) at $T = 5,000$ K which is the mean temperature estimated for [Fe II] line-emitting regions in other SNRs (Graham, Wright, & Longmore 1987; Oliva, Moorwood, & Danziger 1989, ; see also § 4.2). The result is not sensitive to temperature, e.g., a factor of 2 variation in temperature causes 10–20% in density. We adopt the average value $6,600 \pm 900$ cm $^{-3}$ at $T = 5,000$ K as the characteristic electron density of the [Fe II] filaments.

We also detected Br γ line toward [Fe II]-pk1. The dereddened ratio of [Fe II] 1.644 μm to Br γ line is 77_{-10}^{+14} , which is much greater than that ($\lesssim 0.1$) of HII regions but comparable to the ratios observed in other SNRs (see § 4.2).

³Data available at <http://www.astro.princeton.edu/~draine/dust/dustmix.html>.

3.1.3. Proper Motion during 2003–2005

We have two [Fe II] 1.644 μm images taken in 2.2 years apart, i.e., in 2003 June and 2005 August. The time interval is not long enough to notice the proper motion of the [Fe II] filaments in the difference image obtained by subtracting one from the other. We instead inspect one-dimensional intensity profiles of the bright [Fe II] -SE filament to search for its proper motion associated with an expansion.

Fig. 7 shows the intensity profiles across the two bright segments of the [Fe II]-SE filament along the cuts (dashed lines) in Fig. 3. The cuts are made to point to the central pulsar which is very close to the geometrical center of the SNR shell (Kaspi et al. 2001). The distance in the abscissa is measured from the upper right end of the cuts, so that it increases outward from the remnant center. Note that the profiles of the filament in 2005 (solid lines) are slightly shifted outward from those in 2003 (dashed lines). We fit the profiles along the cuts A and B with a Gaussian and obtain shifts of $0.''063 \pm 0.''032$ and $0.''095 \pm 0.''064$ in their central positions, respectively. For comparison, the profiles of nearby stars, e.g., the strong peak at $24''$ in Fig. 7 (left), do not show any appreciable shift. The mean shift in stellar positions from the same 1-dimensional Gaussian analysis of nearby seven stars is found to be $-0.''0067 \pm 0.''0029$. Therefore, the mean proper motion of the SE filament with respect to the nearby stars during 2.2 years amounts to $0.''076 \pm 0.''029$, which corresponds to a rate of $0.''035 \pm 0.''013 \text{ yr}^{-1}$.

3.2. H₂ 2.122 μm emission: Photometry and Spectroscopy

Fig. 8 is a star-subtracted and median-filtered H₂ 2.122 μm image. The image has been made in the same way as Fig. 2. Two small ($\sim 30''$) filaments, one at the southern SNR radio boundary and another fainter one outside the NE boundary are now clearly seen. The one in the southeast (H₂ -SE filament) is bright and elongated along the radio boundary. Its peak surface brightness is $3.0 \pm 0.3 \times 10^{-4} \text{ erg cm}^{-2} \text{ s}^{-1} \text{ sr}^{-1}$ and its flux is $4.3 \pm 0.4 \times 10^{-13} \text{ erg cm}^{-2} \text{ s}^{-1}$. The NE filament (H₂-NE filament) is just outside of the SNR boundary and is located where the radio continuum boundary is distorted. Its surface brightness is $\lesssim 40\%$ of the SE filament peak brightness, while its flux density is $\sim 50\%$ of the SE filament. There is no [Fe II] 1.644 μm emission associated with either H₂ filament. A long ($\sim 2'$) filamentary feature seems to be present well outside the southeastern SNR boundary, but it is too faint to be confirmed.

Fig. 9 shows a detailed structure of the H₂-SE filament. It is composed of two bright segments surrounded by a diffuse envelope. It is just outside of the bright [Fe II]-SE filament,

but there is no apparent correlation between the two (cf. Fig. 3). We have detected two H₂ lines, (1,0) S(1) and (2,1) S(3), toward the peak position of the filament, H₂-pk1 (Fig. 10). Their dereddened ratio, using the column density derived from [Fe II] line ratios ($A_{2.12\mu\text{m}} = 1.59$ mag), is 0.14 ± 0.01 (Table 2), which gives $T_{\text{ex}} \approx 2,100$ K using the transition probabilities of Wolnievicz, Simbotin, & Dalgarno (1998).

4. Discussion

G11.2–0.3 has been proposed to be a young remnant of an SN IIL/b interacting with a dense RSG wind based on its PWN and the small size of the SNR shell (Chevalier 2005). The thick, bright shell is thought to be shocked SN ejecta in contact with shocked wind material. The outer edge of the shell is not sharp and it was suggested that the ambient shock propagating into wind material could be at a larger distance (Green et al. 1988; Chevalier 2005). In the following, we first discuss the physical properties of the H₂ filaments that we have discovered in this paper, and show that our results support the SN IIL/b scenario. Then we discuss the physical properties of the [Fe II] filaments which are thought to be composed of both shocked wind material and shocked SN ejecta.

4.1. H₂ Filaments and Presupernova Circumstellar Wind

4.1.1. Excitation of H₂ filaments

The H₂-SE filament is located at the rim of the bright SNR shell and elongated along the rim, which suggests that it is excited by the SNR shock. The derived $v = 2-1$ excitation temperature ($\approx 2,100$ K) is also typical for shocked molecular gas (Burton, et al. 1989). The dereddened peak H₂ 2.122 μm surface brightness is $1.3 \pm 0.1 \times 10^{-3}$ erg cm⁻² s⁻¹ sr⁻¹, and the dereddened total flux of the SE filament is $1.9 \pm 0.2 \times 10^{-12}$ erg cm⁻² s⁻¹.

The interstellar ultraviolet (UV) photons in principle could excite and heat the H₂ gas to produce similar excitation temperature if the gas is dense enough for collisions to dominate deexcitation (Sternberg & Dalgarno 1989; Burton, Hollenbach, & Tielens 1990). However, the expected H₂ 2.122 μm surface brightness by UV photon excitation is low unless the density is high and the radiation field is very strong, e.g., $n_{\text{H}} \geq 10^5$ cm⁻³ and $G_0 \geq 10^4$ for $\geq 1 \times 10^{-4}$ erg cm⁻² s⁻¹ sr⁻¹ where n_{H} is the number density of H nuclei and G_0 is far UV (FUV) intensity relative to the interstellar radiation field in the solar neighborhood (Burton, Hollenbach, & Tielens 1990). Note that $G_0 = 10^4$ corresponds to an O4-type star at a distance of ~ 1 pc (Tielens 2005). No such strong FUV source exists around the filament.

X-ray emission from the remnant is another source that could possibly excite and heat the H₂ filament. We may consider a molecular clump situated at some distance from an SN explosion. As the SN explodes and the SNR evolves, the X-ray flux increases and, in principle, an ionization-dissociation front may develop and propagate into the clump. If the density is sufficiently high, the H₂ lines from heated molecular gas could show ‘thermal’ line ratios (Gredel & Dalgarno 1995). The H₂ line intensities from such clump depend on details, and no model calculations that may be directly applicable to our case are available (cf. Draine & Woods 1990, 1991; Maloney, Hollenbach, & Tielens 1996). In the following, we instead simply consider the energy budget. If the H₂ 2.122 μm line is emitted by reprocessing the X-ray photons from the SNR falling onto the molecular clump, its luminosity may be written as $L_{2.122} \sim \epsilon L_X (\Omega_{\text{cl}}/4\pi)$ where ϵ is an efficiency of converting the incident X-ray energy flux into H₂ 2.122 μm line emission, L_X is the X-ray luminosity of the remnant, and Ω_{cl} is the solid angle of the clump seen from the SNR center. The above formula is accurate if the clump is small and if the X-ray source is spherically symmetric. Although G11.2–0.3 is not a spherically symmetric source in X-rays, we may use the formula to make a rough estimate of the expected H₂ 2.122 μm line luminosity. The conversion efficiency for SNRs embedded in molecular clouds was calculated to be $\lesssim 1 \times 10^{-3}$ (Lepp & McCray 1983; Draine & Woods 1990, 1991). The efficiency is a function of X-ray energy absorbed per H-nucleon and the above inequality might be valid for X-ray irradiated small clumps too. Now if we assume that the H₂ clump has the line-of-sight extent similar to the extent on the sky (~ 0.5), then $\Omega_{\text{cl}}/4\pi \sim 4 \times 10^{-3}$. Since the X-ray luminosity of G11.2–0.3 is $L_X \sim 10^{36}$ erg s⁻¹ in 0.6–10 keV band (Vasisht et al. 1996), we have $L_{2.122} \lesssim 4 \times 10^{30}$ erg s⁻¹. This is much less than the observed H₂ 2.122 μm luminosity of the SE filament, which is $\sim 6 \times 10^{33}$ erg s⁻¹. Therefore, the X-ray excitation/heating does not appear to be important for the H₂-SE filament.

The above consideration leads us to conclude that the H₂-SE filament is excited by the SNR shock associated with G11.2–0.3. The absence of associated [Fe II] 1.644 μm or Brγ emission suggests that the H₂ emission from the H₂-SE filament might be from warm molecules swept-up by a slow, non-dissociative *C* shock not from reformed molecules behind a fast, dissociative *J* shock. The critical velocity for a shock to be a non-dissociative *C* shock is $\lesssim 50$ km s⁻¹ (Draine, Roberge, & Dalgarno 1983; McKee, Chernoff, & Hollenbach 1984). The dereddened mean surface brightness of the H₂-SE filament is $\sim 8 \times 10^{-4}$ erg cm⁻² s⁻¹ sr⁻¹. This is comparable to the (normal) brightness of a ~ 30 km s⁻¹ shock propagating into molecular gas of $n_{\text{H}} = 10^4$ cm⁻³ according to the *C*-shock model of Draine, Roberge, & Dalgarno (1983). We were unable to find model calculations for lower densities. But, since the intensity will be proportional to the preshock density, provided that the density in the emitting gas is less than the critical density ($\gtrsim 10^5$ cm⁻³; Burton, et al.

1989), the results of Draine, Roberge, & Dalgarno (1983) indicates that a 40–50 km s⁻¹ shock propagating into molecular gas of $n_{\text{H}} = 10^3 \text{ cm}^{-3}$ might have similar (normal) surface brightness. A slower shock with a lower preshock density would be possible if the shock propagating into the H₂ filament is tangential along the line of sight, so that the brightness normal to the shock front is lower.

The situation is not so clear for the H₂-NE filament for which we lack spectroscopic information. Its flux density, however, is comparable to that of the SE filament and we may rule out the excitation by X-rays from G11.2–0.3. We checked 2MASS colors of nearby ($\leq 2'$) stars, but found no OB stars that would be responsible for the UV excitation. This leaves again the shock excitation for the origin of the H₂ emission. A difficulty with the shock excitation is that the filament is located outside the radio SNR boundary. But as have been pointed out in previous studies (e.g., Green et al. 1988), the radio continuum boundary is not sharp and the ambient shock is thought to have propagated beyond the apparent radio boundary. It therefore seems to be reasonable to consider that the H₂-NE filament is excited by the SNR shock too, although we need spectroscopic observations to understand the nature of the H₂-NE filament.

4.1.2. *Circumstellar Origin of H₂ filaments*

The H₂ filaments are more likely of circumstellar origin than interstellar. If interstellar, they must be dense clumps originally in an ambient or parental molecular cloud. We do not expect to observe molecular material around small, young core-collapse SNe in general because massive stars clear out the surrounding medium with their strong UV radiation and strong stellar winds during their lifetime. Some molecular material may survive if the progenitor star is an early B-type (B1–B3) star, which does not have strong UV radiation nor strong stellar winds (McKee, van Buren, Lazareff 1984; Chevalier 1999). A difficulty with this scenario, however, is that then the swept up mass at the current radius (3 pc) is likely to be much greater than the ejecta mass, so that the remnant should have been already in Sedov stage where it would appear as a thin, limb-brightened shell. The thick-shell morphology of G11.2–0.3, however, indicates that it is not yet in Sedov stage. We therefore consider that the H₂ filaments are of circumstellar origin which fits well into the SN IIL/b scenario.

It is plausible that the progenitor of G11.2–0.3 had a strong wind which contains dense clumps. Numerous such clumps have been observed in Cas A, e.g., “Quasi-stationary flocculi (QSF)”, which are slowly moving, dense optical clumps immersed within a smoother wind (van den Bergh 1971; van den Bergh & Kamper 1985). In the 320-yr old Cas A, the shock propagating into the clump is fast (100–200 km s⁻¹; Chevalier & Oishi 2003) while in the

1620-yr old G11.2–0.3 it is slow (30–50 km s⁻¹). Their velocity ratio is comparable to the ratio ($\sim 1/5$) of SNR expansion velocities, which suggests that the winds in G11.2–0.3 and Cas A have similar properties. We may estimate the density contrast between the clump and the smoother wind from the ratio of the shock speed into the clump ($v_c = 30 - 50$ km s⁻¹) to the SNR forward shock speed v_{exp} . If we adopt the result of the radio (20 cm) expansion studies by Tam & Roberts (2003), $v_{\text{exp}} = 1350 \pm 280$ km s⁻¹ so that the density contrast would be $(v_{\text{exp}}/v_c)^2 = 700 - 3,000$. For comparison, Chevalier & Oishi (2003) estimated a density contrast of 3,000 for Cas A.

4.2. [Fe II] Filaments and SN Ejecta

4.2.1. Shock Parameters of the [Fe II]-SE filament

The [Fe II] filaments are located within the bright SNR shell in contrast to the H₂ filaments. The [Fe II]-SE filament has a remarkable correlation with the radio shell in both morphology and brightness. The knotty emission features inside the remnant might be within the shell too, but projected on the sky. The location of the filaments suggests that the [Fe II] emission is almost certainly from the shocked gas. The shock must be radiative and the [Fe II] emission should originate from the cooling layer behind the shock.

The [Fe II]-SE filament is very bright with the dereddened [Fe II] 1.644 μm peak surface brightness of $1.80 \pm 0.18 \times 10^{-2}$ ergs cm⁻² s⁻¹ sr⁻¹. It is in fact the brightest among the known [Fe II] 1.644 μm filaments associated with SNRs. The total dereddened [Fe II] 1.644 μm flux is $1.0 \pm 0.1 \times 10^{-10}$ erg cm⁻² s⁻¹. The ratio of [Fe II] 1.644 μm to Br γ line (~ 80) toward the peak position of the [Fe II]-SE filament is larger or comparable to the ratios observed in other SNRs, e.g., 27 to ≥ 71 in IC 443 (Graham, Wright, & Longmore 1987) or 34 in RCW 103 (Oliva, Moorwood, & Danziger 1989). It was pointed out in previous studies that the high ratio can result from SNR shocks *interacting with the ISM* by the combined effects of ‘shock excitation’ and the enhanced gas-phase iron abundance. First, since the ionization potential of iron atom is only 7.9 eV, FUV photons from the hot shocked gas can penetrate far downstream to maintain the ionization state of Fe⁺ where H atoms are primarily neutral (McKee, Chernoff, & Hollenbach 1984; Hollenbach, Chernoff, & McKee 1989; Oliva, Moorwood, & Danziger 1989). Therefore, [Fe II] lines are emitted mainly in gas with a low degree of ionization at $T = 10^3$ – 10^4 K. This partly explains the observed high ratio of [Fe II] 1.644 μm to Br γ lines, but not all. Shock model calculations showed that the ratio is ~ 1 if the gas-phase iron abundance is depleted as in normal ISM. According to Hollenbach, Chernoff, & McKee (1989), the ratio is ~ 1.5 for shocks at velocities 80–150 km s⁻¹ propagating into a molecular gas of $n_{\text{H}} = 10^3$ cm⁻³ with iron depletion

$\delta_{\text{Fe}} \equiv [\text{Fe}/\text{H}]/[\text{Fe}/\text{H}]_{\odot} = 0.03$ where $[\text{Fe}/\text{H}]_{\odot} = 3.5 \times 10^{-5}$. McKee, Chernoff, & Hollenbach (1984) presented the results on atomic shock calculations including grain destruction: for a 100 km s^{-1} shock propagating into atomic gas of $n_{\text{H}} = 10$ and 100 cm^{-3} , $[\text{Fe II}] 1.2567 \mu\text{m}/\text{H}\beta = 2.7$ and 3.7 with $\delta_{\text{Fe}} = 0.53 - 0.58$ in the far downstream. If we use 0.033 as the ratio of $\text{Br}\gamma$ to $\text{H}\beta$ line intensities which corresponds to a Case B nebula at $5,000 \text{ K}$ (Osterbrock 1989), the ratio corresponds to $[\text{Fe II}] 1.644 \mu\text{m}/\text{Br}\gamma = 80$ and 110 , comparable to the observed ratio. Therefore, gas-phase iron abundance close to the solar is required to explain the observed $[\text{Fe II}] 1.644 \mu\text{m}$ to $\text{Br}\gamma$ ratio toward $[\text{Fe II}]$ -pk1.

The preshock density may be estimated from the $[\text{Fe II}] 1.644 \mu\text{m}$ brightness. The $[\text{Fe II}] 1.644 \mu\text{m}$ surface brightness toward the $[\text{Fe II}]$ -SE filament varies $\sim 1 - 10 \times 10^{-3} \text{ erg cm}^{-2} \text{ s}^{-1} \text{ sr}^{-1}$. Its morphology in Fig. 4 suggests that the shock front might be tangential along the line of sight to enhance the surface brightness of the filament. The normal surface brightness of the 100 km s^{-1} shock propagating into atomic gas of $n_{\text{H}} = 100 \text{ cm}^{-3}$ is $2.5 \times 10^{-4} \text{ erg cm}^{-2} \text{ s}^{-1} \text{ sr}^{-1}$ (McKee, Chernoff, & Hollenbach 1984). It is $0.3 - 2 \times 10^{-3} \text{ erg cm}^{-2} \text{ s}^{-1} \text{ sr}^{-1}$ for $80 - 150 \text{ km s}^{-1}$ shocks propagating into a molecular gas of $n_{\text{H}} = 10^3 \text{ cm}^{-3}$ if the gas-phase abundance of iron was solar (Hollenbach, Chernoff, & McKee 1989). Therefore, the preshock density needs to be $\gtrsim 1,000 \text{ cm}^{-3}$. This appears to be roughly consistent with the electron density derived from $[\text{Fe II}]$ lines ratios. As we pointed out above, the ionization fraction of the $[\text{Fe II}]$ -emitting region is expected to be low. Oliva, Moorwood, & Danziger (1989) estimated a mean ionization fraction of 0.11 , in which case $n_{\text{H}} \approx n_e/0.11 \approx 6 \times 10^4 \text{ cm}^{-3}$. For a 100 km s^{-1} shock, the final compression factor would be ~ 80 (Hollenbach & McKee 1989), so that the above postshock density implies a preshock density of $\sim 800 \text{ cm}^{-3}$. This is close to the density required to explain the surface brightness considering the uncertainties in various parameters. Therefore, a 100 km s^{-1} shock propagating into a gas of $n_{\text{H}} \gtrsim 1,000 \text{ cm}^{-3}$ and destroying dust grains seems to explain the observed parameters of the $[\text{Fe II}]$ -SE filament.

4.2.2. Origin of $[\text{Fe II}]$ filaments

The $[\text{Fe II}]$ filaments could be either shocked circumstellar medium (CSM) or shocked ejecta, or both under the context of the Type IIL/b scenario. In the SE filament, $\text{H I Br}\gamma$ line is detected at the peak position and its ratio to $[\text{Fe II}] 1.644 \mu\text{m}$ line is consistent with a 100 km s^{-1} *interstellar* shock (§ 4.2.1), which implies that the emission is not from metal-rich ejecta but from shocked CSM. For example, when the H_2 clumps in the previous section are swept up by shocked dense ejecta, a stronger shock will propagate into the clumps to dissociate and ionize the gas to produce $[\text{Fe II}]$ emission. Radio observation also suggests

that the remnant is more heavily affected by the ambient medium toward this direction: Kothes & Reich (2001) showed that the magnetic field structure of the bright radio shell is radial in general except the bright SE shell where the degree of polarization is significantly low compared to the other parts of the shell. The non-radial magnetic field and the low degree of polarization suggest that the synchrotron emission is dominated by shocked ambient gas not by shocked ejecta. On the other hand, the SE filament is located in the middle of the radio shell and has a large radial proper motion. If the proper motion is due to expansion of the SNR shell, which is very likely, it implies an expansion velocity of $\geq 830 \pm 310 \text{ km s}^{-1}$ (see next). This suggests that the filament is associated with ejecta. It is possible that some [Fe II] emission originates from dense, Fe-rich ejecta recently swept-up and excited by a reverse shock. We suppose that the [Fe II]-SE filament consists of both the shocked CSM and the shocked ejecta, although it is not obvious how the two interact to develop the observed properties.

The derived proper motion of the [Fe II]-SE filament ($0.''035 \pm 0.''013 \text{ yr}^{-1}$) may be compared to the expansion rate of the radio shell. Tam & Roberts (2003) obtained a mean expansion rate of $0.''057 \pm 0.''012 \text{ yr}^{-1}$ at 1.465 GHz and $0.''040 \pm 0.''013 \text{ yr}^{-1}$ at 4.860 GHz by comparing radio images separated by 17 years. Our proper motion is comparable to the 4.860-GHz expansion rate but is smaller than the 1.465-GHz expansion rate which was considered to be more reliable by the authors. It is possible that the [Fe II]-SE filament is not moving perpendicularly to the sight line, so that the true space motion is greater. But, considering that the filament is located near the boundary of the remnant, the projection effect is probably not large. Instead the difference may be because the proper motion that we have derived in this paper represents the velocity of the brightest portion of the filament while the radio expansion rate might be close to the pattern speed, e.g., the SNR shock speed. Since the velocities of shocked ambient gas and shocked ejecta in the shell might be less than the SNR shock velocity, it is plausible that our ‘expansion rate’ is less than the radio one. We will explore the dynamical properties of G11.2–0.3 in our forthcoming paper.

The [Fe II]-NW filament and the knotty emission features are considered to be mostly, if not all, dense SN ejecta. The radial magnetic field supports this interpretation (Kothes & Reich 2001). Their filamentary and ring-like structure may be a consequence of bubbly Fe ejecta (e.g., Blondin, Borkowski, & Reynolds 2001). It is worth to note that the [Fe II] emission is distributed mainly along the NW-SE direction (Fig. 2), the direction perpendicular to the PWN axis. The long and symmetric morphology of the [Fe II]-SE and -NW filaments resembles the main optical shell of Cas A. Cas A, in optical forbidden lines of O, S ions, shows a complex northern shell composed of several bright, clumpy filamentary structures at varying distances from the center and a relatively simple-structured southern shell (e.g., Fesen 2001). These northern and southern portions of the main optical shell are opposite

across the jet-axis along the NE-SW axis. The optical shell is generally believed to be dense clumps in ejecta recently swept up by reverse shock, although it contains QSFs too. The similarity to Cas A suggests that the explosion in G11.2–0.3 was asymmetric as in Cas A.

The total [Fe II] 1.644 μm luminosity is $\sim 75L_{\odot}$. This is two orders of magnitude greater than Kepler or Crab, but comparable to RCW 103 or IC 443 (Oliva, Moorwood, & Danziger 1989; Keller et al. 1995). In collisional equilibrium at $T = 5,000$ K with $n_e \approx 6,600 \text{ cm}^{-3}$, this converts to Fe mass of $\sim 5.3 \times 10^{-4} M_{\odot}$. Both the shocked ejecta and the shocked CSM constitute this. The ^{56}Fe mass that would have been formed from the radioactive decay of ^{56}Ni in 15–25 M_{\odot} SN explosion is 0.05–0.13 M_{\odot} (Woosley & Weaver 1995; Thielemann, Nomoto, & Hashimoto 1996). Therefore, the Fe ejecta detected in [Fe II] 1.644 μm emission is less than one percent of the total Fe ejecta. On the other hand, the observed Fe mass corresponds to H (+He) mass of 0.27 M_{\odot} for the solar abundance, which implies that the mass of the shocked CSM comprising the Fe filaments should be a tiny fraction of the swept-up CSM too.

5. Conclusion

G11.2–0.3 has been known as an evolved version of Cas A, both being SN IIL/b with a significant mass loss before explosion. Our H_2 results confirm that G11.2–0.3 is indeed interacting with a clumpy circumstellar wind as in Cas A. Clumps with a density contrast of $\sim 3,000$ may be common in presupernova circumstellar wind of SN IIL/b. As far as we are aware, G11.2–0.3 is the first source where the presupernova wind clumps are observed in H_2 emission. The H_2 filament in the northeast is of particular interest because it could provide a strong evidence for an ambient shock beyond the bright radio shell. Future spectroscopic studies will reveal the nature of this filament.

The [Fe II] filaments in G11.2–0.3 are probably composed of both shocked CSM and shocked ejecta. The one in the southeast is the brightest among the known [Fe II] 1.644 μm filaments associated with SNRs and is thought to be where the ejecta is heavily interacting with dense CSM. We note that RCW 103, which is another young remnant of SN IIL/b (Chevalier 2005), has a very bright [Fe II] filament too. The source is similar to G11.2–0.3 in the sense that H_2 emission is detected beyond the apparent SNR boundary, although the H_2 emission in RCW 103 extends along the entire bright SNR shell (Oliva, Moorwood, & Danziger 1990). It is possible that the [Fe II] filaments in the two remnants are of the same origin. The other faint [Fe II]-emitting features of G11.2–0.3 are thought to be mostly SN ejecta. The distribution of [Fe II] filaments suggests that the explosion produced G11.2–0.3 was asymmetric as in Cas A. In Cas A, however, Fe ejecta have been observed mainly in X-rays although faint [Fe II] 1.644 μm lines have been detected toward several fast-moving ejecta

knots from spectroscopic observations by Gerardy & Fesen (2001). Future detailed spectroscopic studies will help us to understand the nature of the [Fe II] filaments and knots in G11.2–0.3 as well as the SN explosion itself.

We thank Dave Green for providing his VLA images of G11.2–0.3. We also wish to thank Chris McKee and Roger Chevalier for their helpful comments. D-SM acknowledges a Millikan fellowship from California Institute of Technology. This work was supported by the Korea Science and Engineering Foundation (ABRL 3345-20031017).

REFERENCES

- Blondin, J. M., Borkowski, K. J., & Reynolds, S. P. 2001, *ApJ*, 557, 782
- Burton, M. G., Brand, P. W. J. L., Geballe, T. R., & Webster, A. S. 1989, *MNRAS*, 236, 409
- Burton, M. G., Hollenbach, D. J., & Tielens, A. G. G. M. 1990, *ApJ*, 365, 620
- Chevalier, R. A. 1999, *ApJ*, 511, 798
- Chevalier, R. A. 2005, *ApJ*, 619, 839
- Chevalier, R. A., & Oishi, J. 2003, *ApJL*, 23
- Cohen, M., Wheaton, Wm. A., Megeath, S. T. 2003, *AJ*, 126, 1090
- Draine, B. T., & Woods, D. T. 1990, *ApJ*, 363, 464
- Draine, B. T., & Woods, D. T. 1991, *ApJ*, 383, 621
- Draine, B. T. 2003, *ARAA*, 41, 241
- Draine, B. T., Roberge, W. G., & Dalgarno, A. 1983, *ApJ*, 264, 485
- Ferland, G. J., Korista, K.T., Verner, D.A., Ferguson, J.W., Kingdon, J.B., Verner, & E.M. 1998, *PASP*, 110, 761
- Fesen, R. A. 2001, *ApJS*, 133, 161
- Fesen, R. A., & Gundersen, K. S. 1996, *ApJ*, 470, 967
- Gerardy, C. L., & Fesen, R. A. 2001, *ApJ*, 121, 2781

- Graham, J. R., Wright, G. S., & Longmore, A. J. 1987, *ApJ*, 313, 847
- Graham, J. R., Wright, G. S., & Longmore, A. J. 1990, *ApJ*, 352, 172
- Gredel, R., & Dalgarno, A. 1995, *ApJ*, 446, 852
- Green, D. A. 2004, *Bull. Astron. Soc. India*, 32, 335
- Green, D. A., Gull, S. F., Tan, S. M., & Simon, A. J. B., 1988, *MNRAS*, 231, 735
- Hanson, M. M., Conti, P. S., & Rieke, M. J. 1996, *ApJS*, 107, 281
- Hartigan, P., Raymond, J., & Pierson, R. 2004, *ApJL*, 614, 69
- Hollenbach, D., & McKee, C. F. 1989, *ApJ*, 342, 306
- Hollenbach, D., Chernoff, D. F., & McKee, C. F. 1989, in *Proceedings of the 22nd Eslab Symposium*, ed. B.H. Kaldeich (ESA SP-290; European Space Agency), 245
- Hwang, U., & Laming, J. M. 2003, *ApJ*, 597, 362
- Hwang, U. et al. 2004, *ApJL*, 615, 117
- Kaspi, V. M., Roberts, M. E., Vasisht, G., Gotthelf, E. V., Pivovarov, M., & Kawai, N. 2001, *ApJ*, 560, 371
- Keller, L. D., Jaffe, D. T., Pak, S., Luhman, M. L., Claver, C. F. 1995, *Rev. Mexicana Astron. Astrofis. Ser. Conf.* 3, 251
- Kothes, R., & Reich, W. 2001, *A&A*, 372, 627
- Larkin, J. E., Knop, R. A., Lin, S., Matthews, K., & Soifer, B. T. 1996, *PASP*, 108, 211
- Lee, H.-G. 2005, *JKAS*, 38, 385
- Lepp, S., & McCray, R. 1983, *ApJ*, 269, 560
- Livingston, W. & Wallace, L. 1991, N.S.O. Technical Report #91-001
- Maiolino, R., Rieke, G. H., & Rieke, M. J. 1996, *AJ*, 111, 537
- Maloney, P. R., Hollenbach, D. J., & Tielens, A. G. G. M. 1996, *ApJ*, 466, 561
- McKee, C. F., Chernoff, D. F., & Hollenbach, D. J. 1984, in *Galactic and Extragalactic Infrared Spectroscopy*, eds. M. F. Kessler, J. P. Phillips (Reidel; Dordrecht), 103

- McKee, C. F., Van Buren, D., & Lazareff, B. 1984, *ApJL*, 278, 115
- Nussbaumer, H., & Storey, P. J. 1988, *A&A*, 193, 327
- Oliva, E., Moorwood, A. F. M., & Danziger, I. J. 1989, *A&A*, 214, 307
- Oliva, E., Moorwood, A. F. M., & Danziger, I. J. 1990, *A&A*, 240, 453
- Osterbrock, D. E. 1989, *Astrophysics of Gaseous Nebulae and Active Galactic Nuclei* (University Science Books, Mill Valley)
- Padhan, A. K., & Zhang, H. L. 1993, *ApJ*, 409, L77
- Quinet, P., Le Dourneuf, M., & Zeippen, C. J. 1996, *A&AS*, 120, 361
- Reach, W. T. et al. 2006, *AJ*, in press
- Roberts, M. S. E. et al. 2003, *ApJ*, 588, 992
- Rousselot, P., Lidman, C., Cuby, J.-G., Moreels, G., & Monnet, G. 2000, *A&A*, 354, 1134
- Smith, N., & Hartigan, P. 2006, *ApJ*, 638, 1045
- Stephenson, F. R., & Green, D. A. 2002, *Historical Supernovae and their Remnants* (Clarendon Press, Oxford)
- Sternberg, A., & Dalgarno, A. 1989, *ApJ*, 338, 197
- Tam, C., & Roberts, M. S. E. 2003, *ApJL*, 598, 27
- Thielemann, F.-K., Nomoto, K., & Hashimoto, M.-A. 1996, *ApJ*, 460, 408
- Tielens, A. G. G. M. 2005, *The Physics and Chemistry of the Interstellar Medium* (Cambridge: Cambridge Univ. Press)
- Vacca, W. D., Cushing, M. C., & Rayner, J. T. 2003, *PASP*, 115, 389
- van den Bergh, S. 1971, *ApJ*, 165, 457
- van den Bergh, S., & Kamper, K. 1985, *ApJ*, 293
- Vasisht, G., Aoki, T., Dotani, T., Kulkarni, S. R., & Nagase, F. 1996, *ApJL*, 456, 59
- Wolniewicz, L., Simbotin, I., & Dalgarno, A., 1998, *ApJS*, 115, 293
- Woosley, S. E. & Weaver, T. A. 1995, *ApJS*, 101, 181

Young, P. A. et al. 2006, ApJ, 640, 891

Zhang, H. L., & Pradhan, A. K. 1995, A&A, 293, 953

Table 1. Summary of WIRC Imaging Observations of G11.2-0.3

Filter	$\lambda_{\text{center}}^a$ (μm)	$\Delta\lambda_{\text{equiv}}^b$ (μm)	Exposure (s)	NDI ^c	Date
[Fe II] ^d	1.644	0.0252	60	12	2003. 06. 17, 2005. 08. 27
H ₂	2.120	0.0329	20	36	2005. 08. 14
Br γ	2.166	0.0327	30	20	2005. 08. 28
<i>K</i> _s	2.150	0.312	15	90	2003. 06. 16
<i>H</i> -cont	1.570	0.0236	30	10	2005. 08. 14
<i>K</i> -cont	2.270	0.0330	60	12	2005. 08. 27

^aWavelength centers from http://www.astro.caltech.edu/palomar/200inch/wirc/wirc_spec.html

^bEquivalent width, e.g, $\Delta\lambda_{\text{equiv}} = \int S(\lambda)d\lambda$ where $S(\lambda)$ is the normalized filter response.

^cNDI represents “number of dithered images.”

^dThere are two observations with [Fe II] filter: one in 2003 and the other in 2005. The observing parameters are the same for the two observations.

Table 2. Detected Lines and Their Strengths

Position	Wavelength ^a	Transition	Relative Strength ^b	
			Observed	Dereddened
[Fe II] -pk1 ^c	1.2567	[Fe II] a ⁴ <i>D</i> _{7/2} → a ⁶ <i>D</i> _{9/2}	0.314 (0.010)	1.04
	1.5335	[Fe II] a ⁴ <i>D</i> _{5/2} → a ⁴ <i>F</i> _{9/2}	0.116 (0.004)	0.151 (0.005)
	1.5995	[Fe II] a ⁴ <i>D</i> _{3/2} → a ⁴ <i>F</i> _{7/2}	0.102 (0.003)	0.113 (0.003)
	1.6436	[Fe II] a ⁴ <i>D</i> _{7/2} → a ⁴ <i>F</i> _{9/2}	1.0	1.0
	1.6638	[Fe II] a ⁴ <i>D</i> _{1/2} → a ⁴ <i>F</i> _{5/2}	0.052 (0.002)	0.050 (0.002)
	2.1661	H 4-7 Br γ	0.030 (0.004)	0.013 (0.002)
H ₂ -pk1 ^d	2.0735	H ₂ (2-1) S(3)	0.13 (0.01)	0.14 (0.01)
	2.1218	H ₂ (1-0) S(1)	1.0	1.0

^aRest wavelengths of the identified lines.

^bLine fluxes relative to the [Fe II] 1.644 μm flux for [Fe II]-pk1 and relative to H₂ 2.122 μm flux for H₂-pk1. The numbers in parentheses are 1σ statistical errors. The observed [Fe II] 1.644 μm surface brightness at [Fe II]-pk1 is $1.9(0.2) \times 10^{-3}$ erg cm⁻² s⁻¹ sr⁻¹ and H₂ 2.122 μm surface brightness at H₂-pk1 is $3.0(0.3) \times 10^{-4}$ erg cm⁻² s⁻¹ sr⁻¹ according to our narrow-band imaging photometry.

^cThe coordinate of the [Fe II] 1.644 μm peak position is (18^h 11^m 34.^s76, −19° 26′ 30.[″]0). The slit was slightly off from the peak position and the spectrum was extracted from a 3″ × 1″ area (P.A.=38°) centered at ($\Delta\alpha, \Delta\delta$) = (+1.[″]4 ± 0.[″]2, −0.[″]8 ± 0.[″]2) from the peak position (see Fig. 3).

^dThe coordinate of the H₂ 2.122 μm peak position is (18^h 11^m 32.^s26, −19° 27′ 10.[″]5). The slit was slightly off from the peak position and the spectrum was extracted from a 3″ × 1″ area (P.A.=59°) centered at ($\Delta\alpha, \Delta\delta$) = (+0.[″]5 ± 0.[″]5, −0.[″]5 ± 0.[″]5) from the peak position (see Fig. 9).

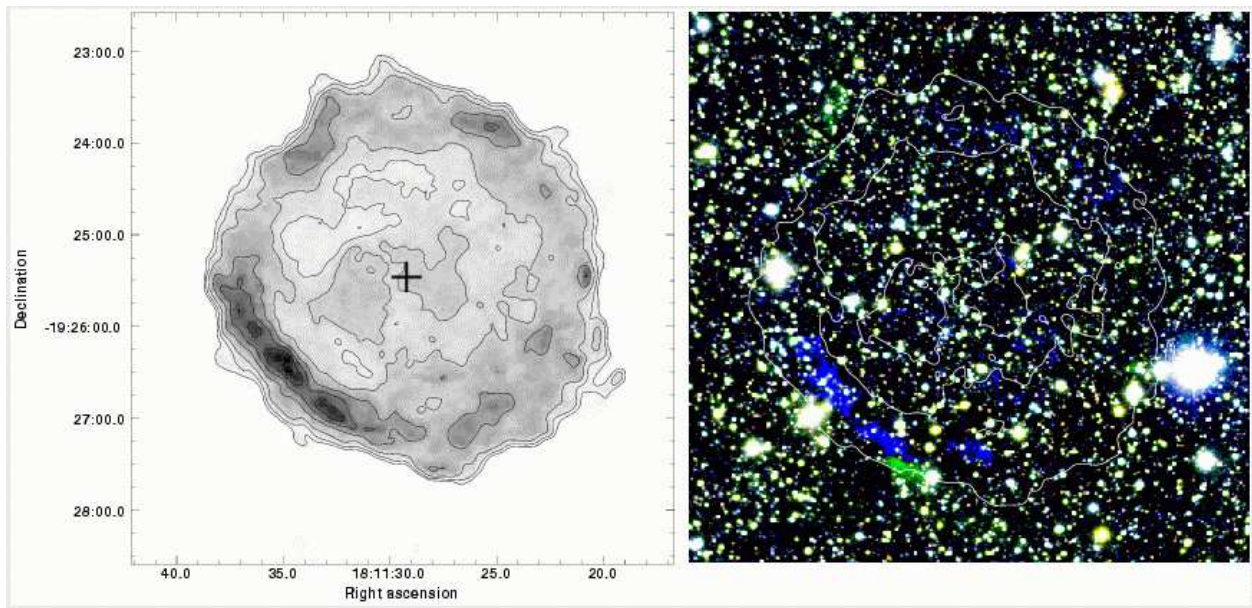


Fig. 1.— Near infrared image compared with radio map of G11.2–0.3. Left panel: VLA 1.4 GHz map from Green et al. (1988). The cross marks the position of pulsar. Contour levels are 0.5, 1, 2, 3, 4, 6, and 8 mJy/pixel where the pixel size is $1.''4 \times 1.''4$. Right panel: Three color image generated from [Fe II] $1.644 \mu\text{m}$ (B), H_2 $2.122 \mu\text{m}$ (G), and $\text{Br}\gamma$ $2.166 \mu\text{m}$ (R). The 2 mJy/pixel radio contours are overlaid to mark the SNR shell.

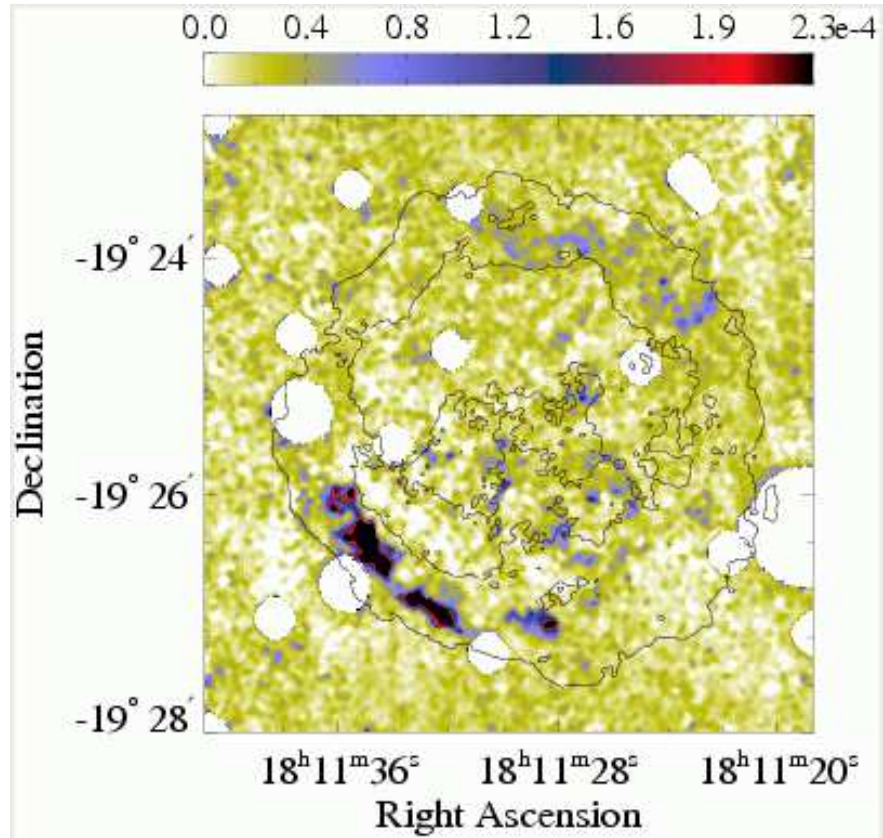


Fig. 2.— [Fe II] $1.644 \mu\text{m}$ image with stars subtracted using PSF photometry. Bright stars are masked out and a median smoothing filter is applied to remove faint stars (see text for details). Color bar is given at the top of the image in units of $\text{erg cm}^{-2} \text{s}^{-1} \text{sr}^{-1}$. The 2 mJy/pixel radio contours are overlaid.

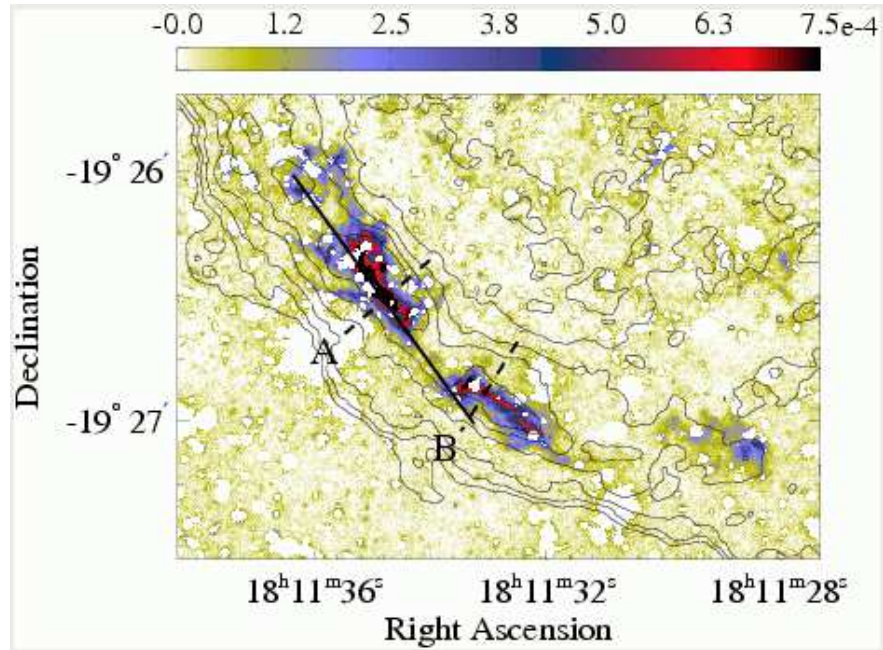


Fig. 3.— An enlarged [Fe II] $1.644 \mu\text{m}$ image of the [Fe II]-SE filament. Stars are just masked out using a continuum image in order to avoid any artifacts in the PSF star-subtraction. Color bar is given at the top of the image in units of $\text{erg cm}^{-2} \text{s}^{-1} \text{sr}^{-1}$. The thick solid line shows the slit position for spectroscopy, while the thick dashed lines labeled ‘A’ and ‘B’ mark the cuts over which the intensity profiles in Fig. 7 are obtained. Radio contours are overlaid.

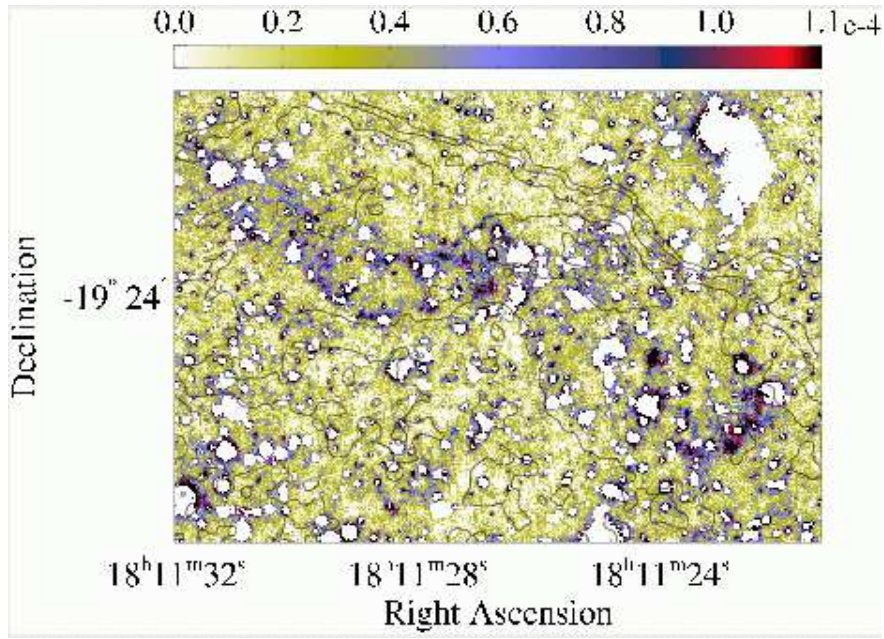


Fig. 4.— An enlarged [Fe II] 1.644 μm image of the [Fe II]-NW filament. See the caption in Fig. 3 for explanation.

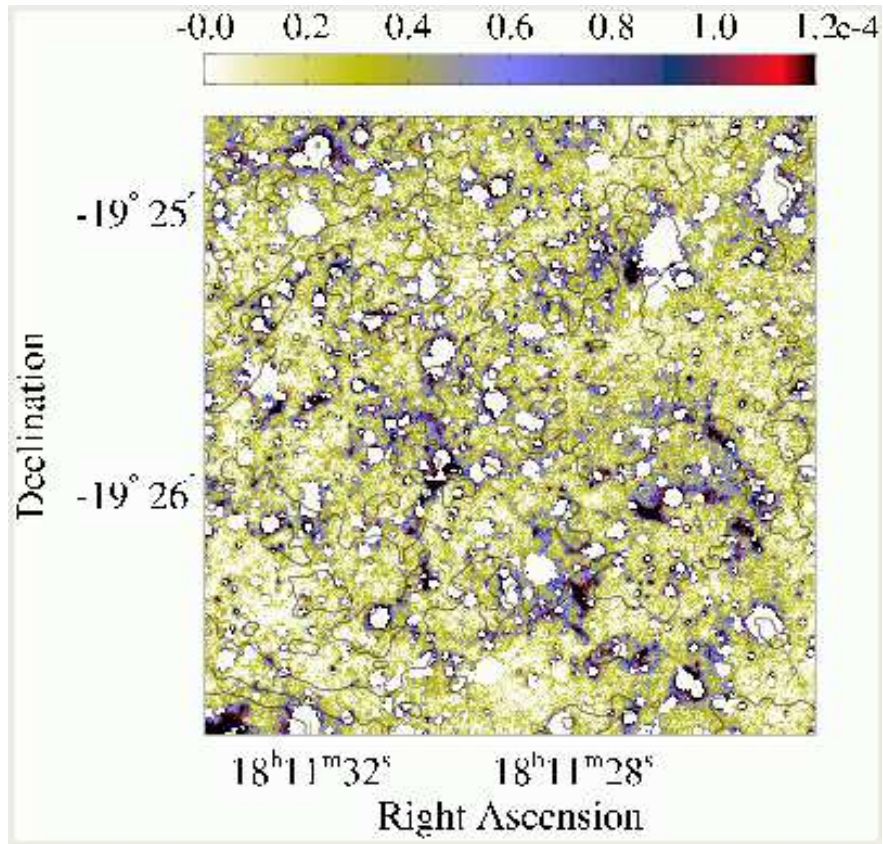


Fig. 5.— An enlarged [Fe II] 1.644 μm image of the central SNR area. See the caption in Fig. 3 for explanation.

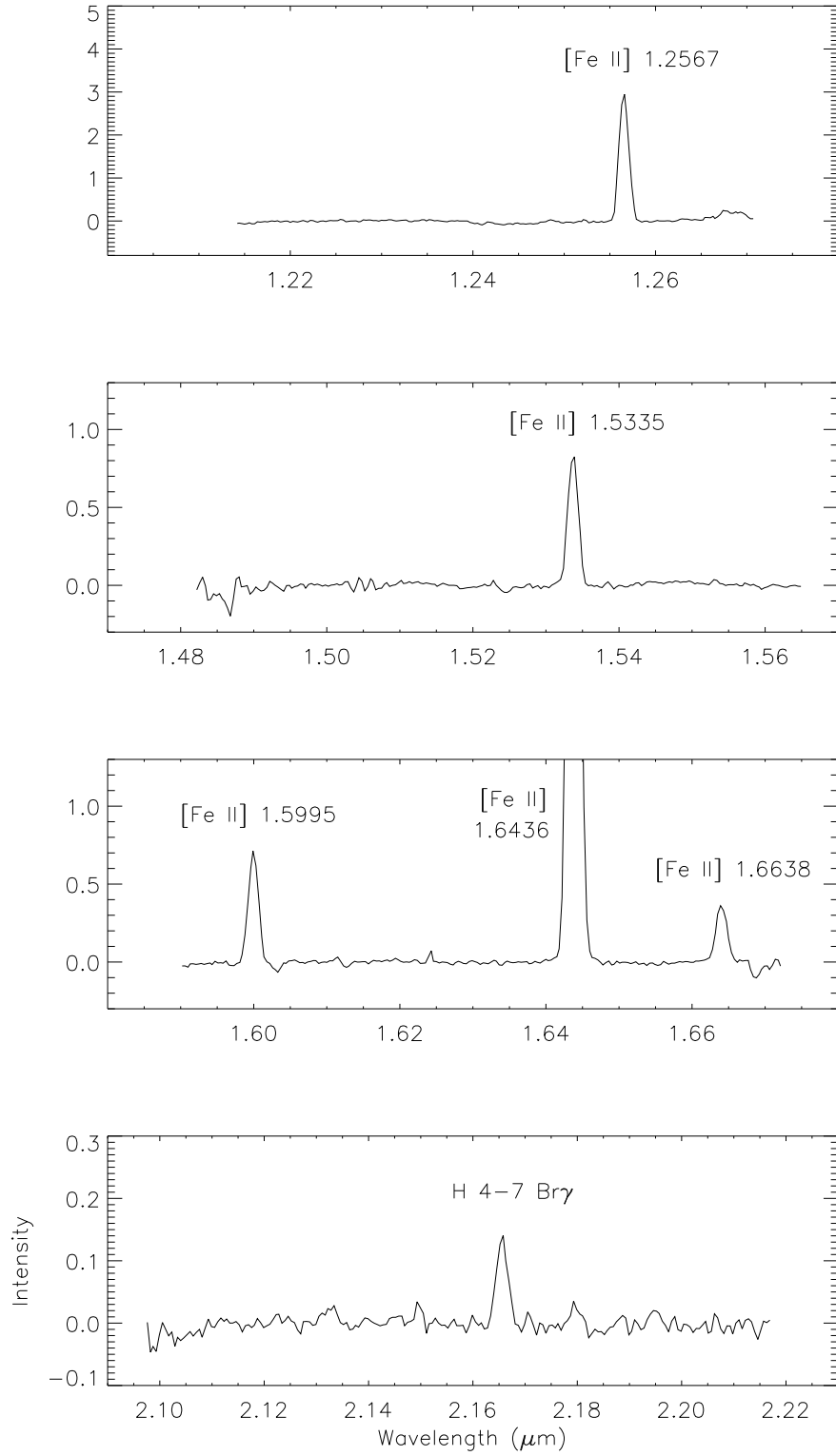


Fig. 6.— [Fe II] and Br γ spectra of [Fe II]-pk1. The intensity is in arbitrary scale. The peak intensity of the [Fe II] 1.644 μm line is 6.9 in this scale.

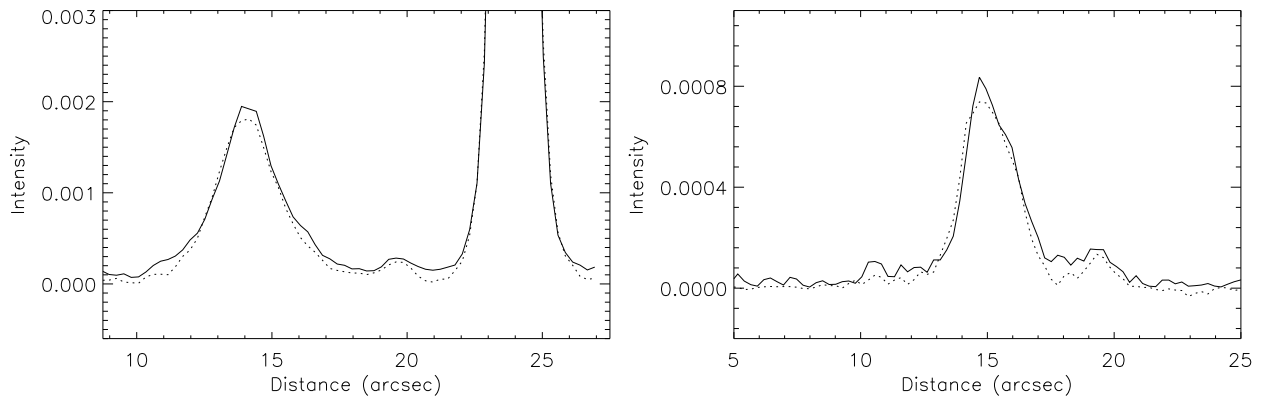


Fig. 7.— Comparison of the brightness distribution of the [Fe II]-SE filament in 2005 (solid lines) and that in 2003 (dotted lines). Left and right figures show the distribution across the two bright segments of the [Fe II]-SE filament along the cuts labeled ‘A’ and ‘B’ in Fig. 3, respectively. The distance in the abscissa is measured from the upper right end of the cuts, so that it increases outward from the remnant center. Note that the profiles of the filament in 2005 are slightly shifted outward from those in 2003.

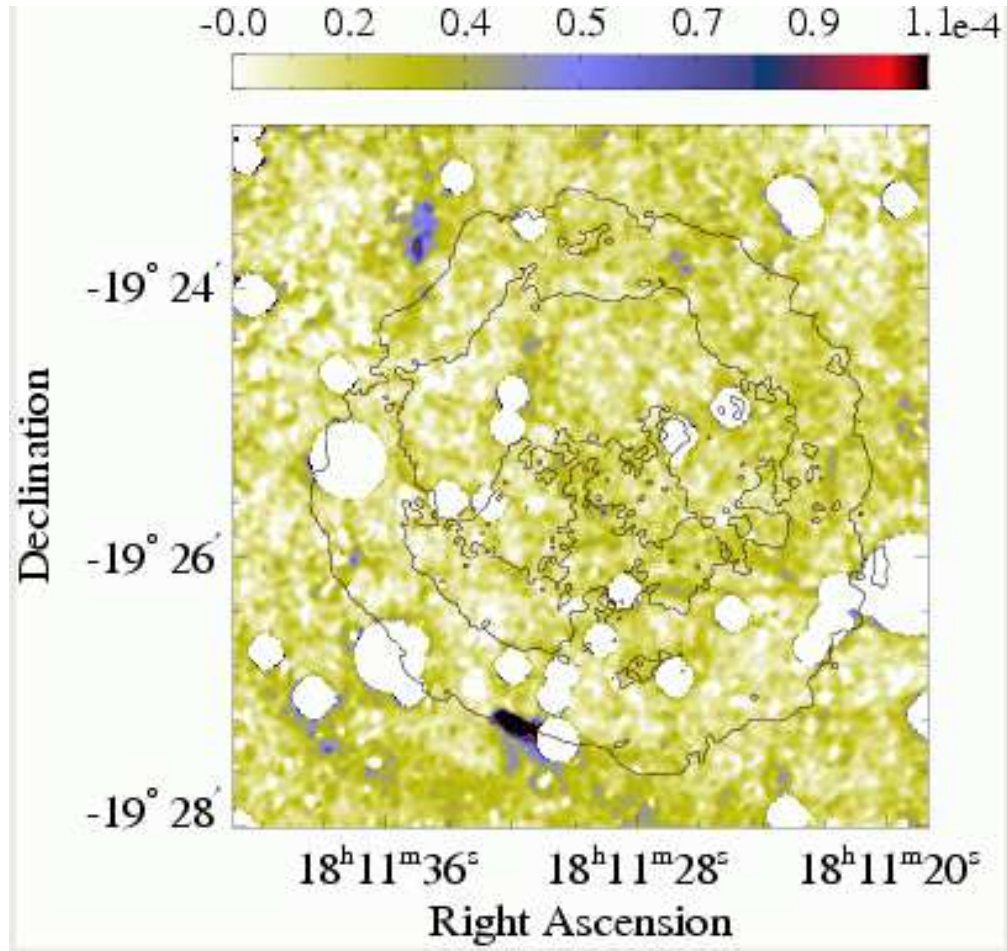


Fig. 8.— Same as Fig. 2, but for H₂ emission.

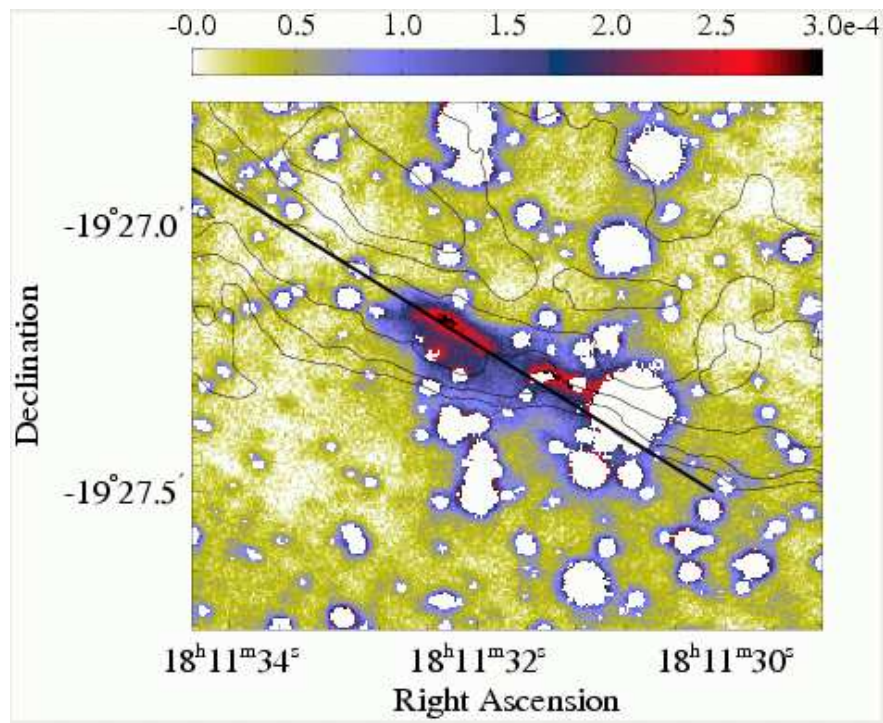


Fig. 9.— An enlarged H₂ 2.122 μm image of the H₂-SE filament. See the caption in Fig. 3 for explanation.

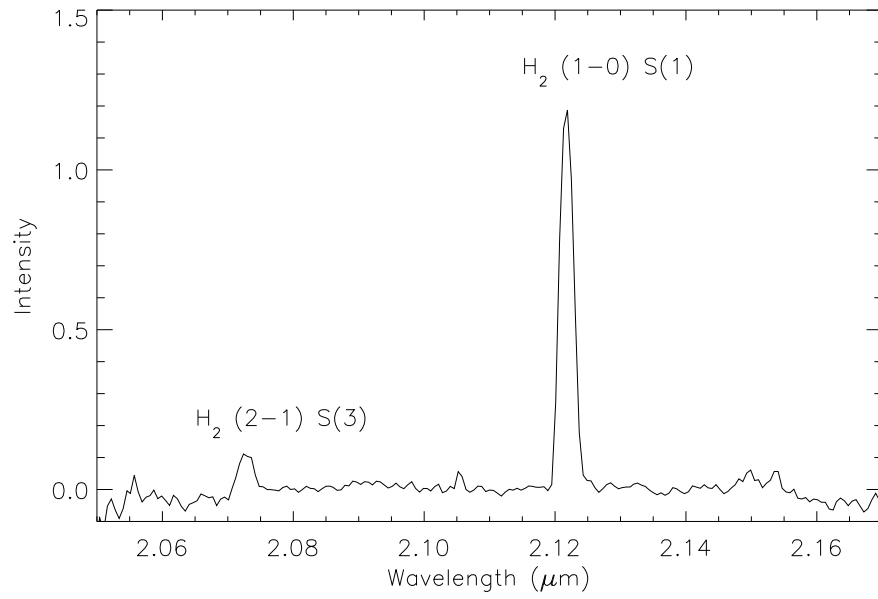


Fig. 10.— H₂ spectra of H₂-pk1. The intensity is in arbitrary scale.